Li, X., Lucas, M. and Harkness, P. (2018) Full and half-wavelength ultrasonic percussive drills. *IEEE Transactions on Ultrasonics, Ferroelectrics, and Frequency Control*, (doi:10.1109/TUFFC.2018.2867535)

This article has been accepted for publication in a future issue of this journal, but has not been fully edited. Content may change prior to final publication. Citation information: DOI 10.1109/TUFFC.2018.2867535, IEEE Transactions on Ultrasonics, Ferroelectrics, and Frequency Control

Full and half-wavelength ultrasonic percussive drills

Xuan Li, Margaret Lucas, Patrick Harkness*

School of Engineering, University of Glasgow, Glasgow, G12 8QQ, UK

Abstract

Ultrasonic-percussive drills are a leading technology for small rock drilling applications where power and weight-on-bit are at a premium. The concept uses ultrasonic vibrations to excite an oscillatory motion in a free-mass, which then delivers impulsive blows to a drilling-bit. This is a relatively complex dynamic problem involving the transducer, the free-mass, the drilling-bit and, to a certain extent, the rock surface itself. This paper examines the performance of a full-wavelength transducer compared to a half-wavelength system, which may be more attractive due to mass and dimensional drivers. To compare the two approaches, three-dimensional finite element models of the ultrasonic-percussive stacks using full and half wavelength ultrasonic transducers are created to assess delivered impulse at similar power settings. In addition, impact-induced stress levels are evaluated to optimize the design of drill tools at a range of internal spring rates before, finally, experimental drilling is conducted. The results suggest that full-wavelength systems will yield much more effective impulse but, interestingly, their actual drilling performance was only marginally better than half-wavelength equivalents.

Keywords: ultrasonic-percussive, effective impulse, planetary drilling

1. Introduction

Conventional drilling techniques often have force, torque, power, and mass [1] requirements that are incompatible with lightweight spacecraft in low-gravity environments. Ultrasonic percussion [2], [3] is a step towards addressing this issue, and drill testbeds such as the UPCD (Ultrasonic Planetary Core Drill) have a full wavelength ultrasonic transducer consisting of a back-mass, piezoelectric elements and a step-horn [3] with a gain of eight.

The objective of this research is to determine whether a smaller half-wavelength ultrasonic stack can deliver comparable performance, combined with the additional benefits of a reduction in the scale and mass of the device. The half-wavelength ultrasonic percussive stack uses a single-piece ultrasonic element with a gain of 4.6 [4].

Both ultrasonic transducers operate at 20kHz, and both use the same ultrasonic-percussive technique where ultrasonic vibrations at the transducer-horn tip excite a free-mass, which oscillates chaotically at around 1kHz [5]. The motion is constrained by pressure from the front and rear springs, but concentrates energy into impacts upon the drill-bit, and hence to the bit/rock interface, where the rock fractures when the applied pressure exceeds its compressive strength. In order to assess theoretical rate-of-progress, a term called 'effective impulse' is defined, which is the time-integral of applied force above the compressive strength threshold [6].

The configuration of both devices is based on a commercial transducer (Sonic Systems L500) and a generator (Sonic Systems P100), as shown in **Fig. 1 (a)** and **Fig. 1 (b).** Both drill tools contain three rear spiral springs on vertical shafts, which are balanced axially by a front wave spring around the lance. The free-mass sits on a shaft, where its oscillations transfer energy to the lance and hence on to the drill-bit, while the drill-bit itself is keyed into a spline bearing housed in a cog gear driven by a Maxon DC motor [7]. Rotation of the drill-bit avoids imprintation of the tungsten carbide cutting teeth and allows debris to be augered out of the hole. According to the mechanical design, the full wavelength drill tool shown in **Fig. 1 (a)** has a mass of 3.12kg, while the half wavelength drill tool in **Fig. 1 (b)** has a mass of 2.43kg.

Saving almost 1kg of mass on the surface of Mars corresponds to saving many tens of kilograms in Earth orbit, which in turn corresponds to saving further orders of magnitude of take-off mass and, hence, realises a reduction in the mission costs. A considerable reduction in length is also achieved for the half wavelength drill tool which means that there are further benefits to leverage, particularly with respect to the demands placed upon the atmospheric entry package.

To determine if the full wavelength drill tool, which has already been field-tested at a Mars analogue site in Antarctica [8], can indeed be compressed to a half-wave system, a study on the dynamic behaviour of both drill tool configurations is now reported.

2. Ultrasonic transducers

The ultrasonic transducers employed in the drill tools are standard Bolted Langevin-style Transducers (BLT), which consist of a pair of piezoceramic rings sandwiched between a back mass and a front mass, as shown in **Fig. 2**. In this study, the piezoceramic material is PZT-8 Navy type III and the metal masses used are Grade 5 Ti-6Al-4V titanium alloy.

In previous research [9], the ultrasonic transducer was

This research has received funding from the European Union's Seventh Framework Programme (FP7/2007-2013) under Grant Agreement No. 607015. Corresponding author: Dr. Patrick Harkness (email: Patrick.Harkness@glasgow.ac.uk)

This article has been accepted for publication in a future issue of this journal, but has not been fully edited. Content may change prior to final publication. Citation information: DOI 10.1109/TUFFC.2018.2867535, IEEE Transactions on Ultrasonics, Ferroelectrics, and Frequency Control

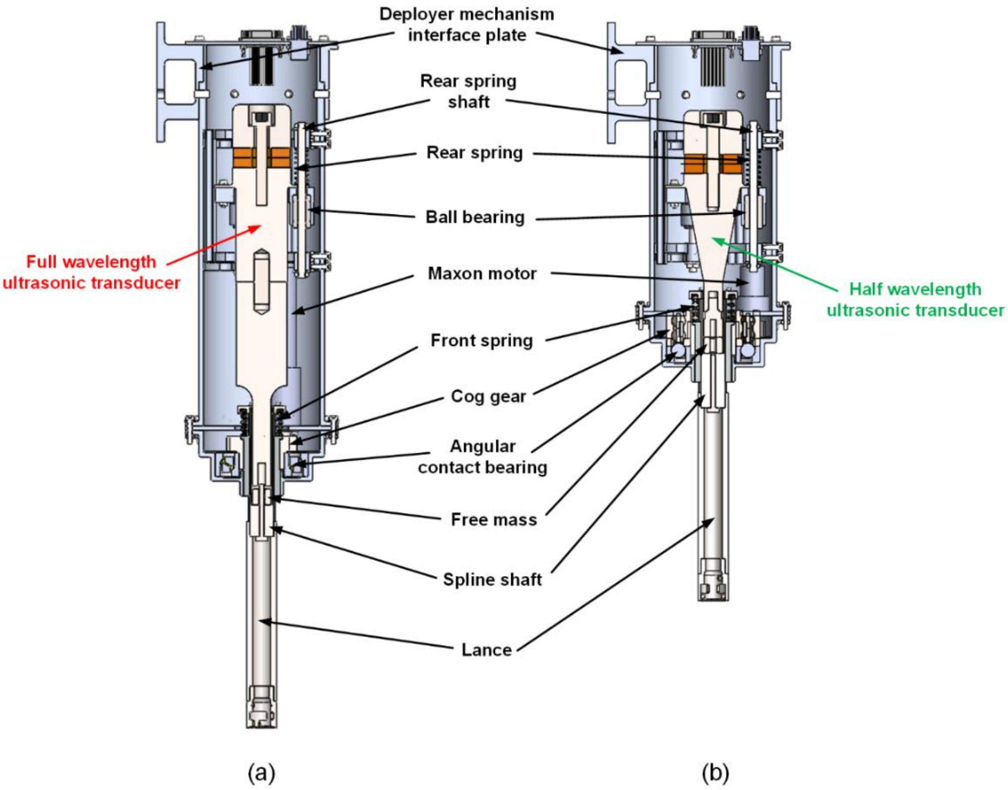

Fig. 1 Cross-sectional views of the drill tools: (a) with a full wavelength transducer, (b) with a half wavelength transducer

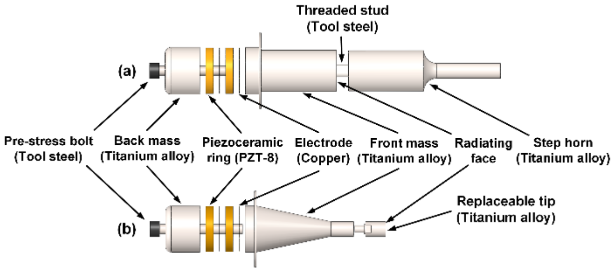

Fig. 2 Exploded views of the ultrasonic transducers. (a) full wavelength, (b) half wavelength.

represented as a one-dimensional mass-spring-damper (MSD) analytical model in Matlab-Simulink. The validity of the one-dimensional model relied on the identification of parameters of the mechanical components, such as stiffness, damping coefficient, and effective mass. However, to fully understand the dynamic behaviour of the three-dimensional drill tools, a Finite Element Analysis (FEA) is now performed, with Experimental Modal Analysis (EMA) and Impedance Analysis (IA) for validation (**Figs. 3-4**).

2.1 Finite Element Analysis of the transducers

Abaqus-Simulia software (Dassault Systèmes) is used for the FE analysis, with the piezoelectric properties of the piezoceramic rings extracted from the manufacturer's data (Morgan Electro Ceramics) [10]. Analyses are conducted to obtain the modal parameters, the vibration amplitude response, and the electrical impedance-frequency response.

2.2 Experimental modal analysis of the transducers

Experimental modal analysis is a data acquisition and visualisation process which uses experimentally-obtained Frequency Response Functions (FRF) to capture the modal parameters (modal frequency, modal damping, and mode shape) [11]. For the two transducers studied here, a forced excitation is adopted with a flat power spectrum across the frequency band of interest [12]. This band of interest in this case is 0kHz to 50kHz, capturing the behaviour around the 20kHz operating mode.

The excitation is generated by a signal generator (Data Physics Quattro) and amplified by a power amplifier (QSC RMX 4050HD), before being supplied to the ultrasonic transducers. A 3-D laser vibrometer (Polytec CLV3000) is used to measure the vibrational velocities at a grid of points on the target surface. Data acquisition and processing software (SignalCalc, Data Physics) are employed to calculate the Frequency Response Functions (FRF) from the input and output signals of the ultrasonic transducer and to apply curve-fitting routines to extract the frequency, magnitude and phase data.

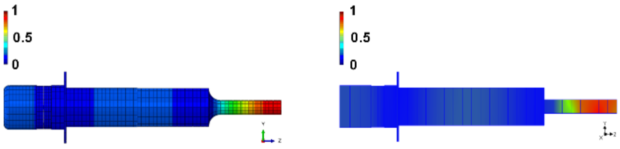

(a) 2nd L-Mode FEA (19833Hz)

(b) 2nd L-Mode EMA (19806Hz)

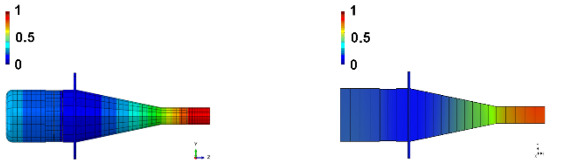

(c) 1st L-Mode FEA (19811Hz)

(d) 1st L-Mode EMA (20353Hz)

Fig. 3 FEA and EMA for the normalized 2nd longitudinal (operating) mode of the full wavelength transducer (a), (b); and 1st longitudinal (operating) mode of the half wavelength transducer (c), (d).

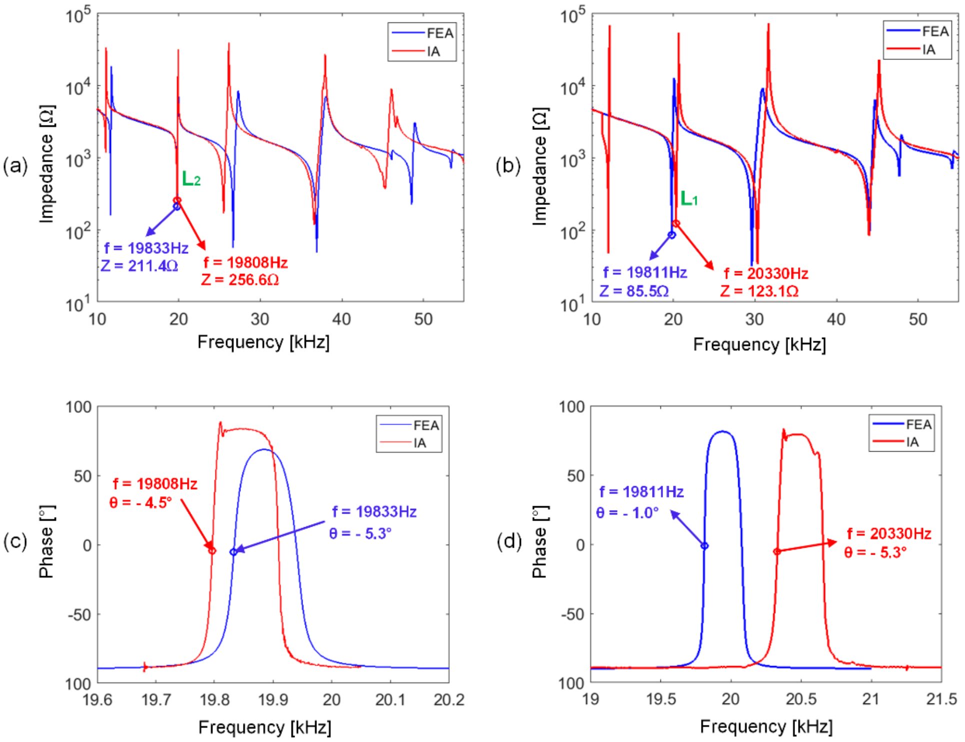

Fig. 4 Electrical impedance of the full wavelength (a) and half wavelength transducers (b), and corresponding phase angles for the full wavelength (c) and half wavelength (d) systems, using FEA and IA.

Finally, the measured velocity data points are exported to the modal analysis software (ME'scopeVES, Vibrant Technology Inc), in order to extract the eigen-modes.

In order to compare the predicted and experimentally extracted mode shapes, the operating longitudinal modes for both ultrasonic transducers are shown in **Fig. 3**. For the full wavelength ultrasonic transducer the operating mode is the 2nd longitudinal mode and for the half wavelength transducer it is the 1st longitudinal mode.

The correlation in mode shapes and resonant frequencies between the FEA and EMA results suggest that these models capture the behaviour of the transducers well, and may now be taken forward to better understand the real electromechanical transducers dynamic characteristics.

2.3 Impedance analysis of the transducers

The electrical characteristics are also analysed. In FEA, the impedance-frequency response was obtained by calculating the derivative of the concentrated charge at piezoceramic ring surfaces and then dividing by the supplied voltage. In experiment, the impedance-frequency response of the transducers was measured using an impedance analyser (Agilent 4395A). The frequency increment was 0.5Hz, while the input AC voltage to the piezoceramic rings was maintained at 1V root mean square (rms) potential to the ground.

The predicted electrical impedances in FEA, as well as the measured impedances, for both full wavelength and half wavelength ultrasonic transducers are presented in **Fig. 4**.

Both full wavelength and half wavelength ultrasonic transducers present minor phase angles θ in the electrical impedance at the operating resonances. This means that the electromechanical ultrasonic transducers will present nearly pure resistive behavior at resonances, where the applied AC voltage to the piezoceramic rings and the generated AC current will be almost in-phase. In other words, the supplied power to the piezoceramic rings will be consumed to contribute to the generation of mechanical vibrations, and very little will be expended to compensate for the minor phase shift between voltage and current.

3. Experimental parametric study of the ultrasonic percussive stacks

A number of percussive hammering experiments were performed. **Fig. 5** shows the experimental rig, testing the full wavelength architecture.

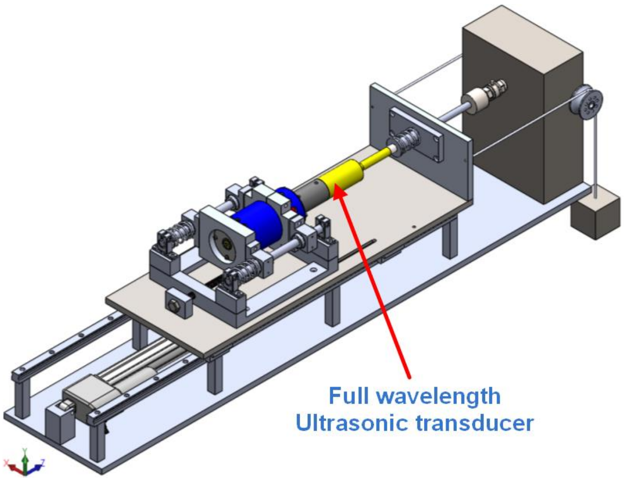

Fig. 5 Full wavelength percussive stack in the test rig.

The ultrasonic-percussive drills are seated between a front spring and two parallel rear springs, which apply an internal pre-load between the ultrasonic transducer, free-mass and drill-bit, so that the ultrasonic percussion can be triggered in free air rather than by applying an external loading to activate percussion. At the tip of the drill-bit, an impact plate made of Grade 5 Ti-6Al-4V alloy is attached to a force sensor (Kistler 9321B), which backs onto a heavy stanchion.

The drill tool assembly can be driven along the horizontal rails by two parallel sets of equal weights applied through two pulley wheels attached on the stanchion, providing the experimental weight-on-bit.

Previous research [9] on the full wavelength drill tool suggested that a minor change in the mass of the free-mass, within a specified range, will not significantly affect the delivered impulse to the impact plate, and consequently a 6g toroidal free-mass is selected. For the drill-bit, it was found that a similar level of impulse was delivered to the impact plate using one drill-bit or multiple connected drill-bits, and therefore a single drill-bit element (80g) is used throughout. However, varying front and rear spring rates can considerably influence the delivered impulse. The available springs in these experiments are [5.00, 10.05, 14.95, 19.90] N/mm for the front springs and [5.10, 10.00, 15.02, 19.98] N/mm for the rear springs.

3.1 Ultrasonic power of percussion, in air, for both percussive stacks

We recall that the aim of this paper is to compare the percussion performance for both drill tools in terms of delivered impulse to the target surface, for the same set of mechanical parameters and a similar level of acoustic power consumption.

Therefore, it is important to ensure the ultrasonic power consumption is consistent for both full and half wavelength transducers before percussion is triggered. Fig. 4 (c) and (d) show that the phase difference between the supplied voltage and developed current in the piezoceramic rings for both ultrasonic transducers is minor, which ensures the input power to both drill tools is equivalent. In experiments, a 5μm peak-to-peak ultrasonic transducer excitation level is selected to activate the full wavelength system, which develops 1.97W of ultrasonic power in free air. For the half wavelength ultrasonic transducer, a 5.9 μm peak-to-peak vibration excitation is selected which develops 1.95W of power in free air, giving an equivalent power level for comparison of the drill tools performance.

The internal pre-load for the full wavelength drill tool is set to approximately 10N when varying the front and rear spring stiffness values in experiments. To achieve the same level of power consumption for the half wavelength percussive drill in air, its internal pre-load is adjusted to match to the full wavelength drill tool percussion in air.

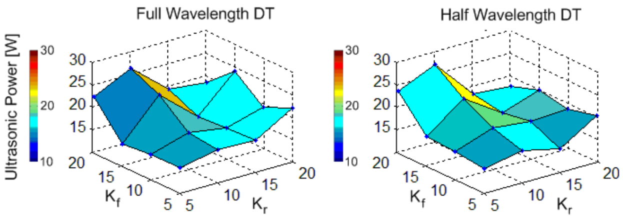

Fig. 6 Measured ultrasonic power for both percussive stacks during percussion in air: k_f – front spring rate (N/mm), k_r – rear spring rate (N/mm)

After this adjustment has been made, ultrasonic power is recorded for 5 seconds percussion in air using a data acquisition unit (PicoScope 4424) and the average power is calculated. The results, presented in **Fig. 6**, show that the full and half wavelength systems have been successfully set up to consume approximately equivalent power across the entire parameter space in question.

3.2 Effective impulse evaluation of the percussive stacks

With consistent ultrasonic power consumption established, weight-on-bit of 5N, 10N and 15N are applied in order to evaluate the delivered momentum. The hammering force is recorded for 5 seconds in each test.

Next, in order to calculate the effective impulse [6], a force threshold needs to be prescribed. This threshold is broadly proportional to the local impact pressure required to exceed the compressive strength of a certain type of rock in order to fracture it. Four force threshold levels were chosen to evaluate the delivered impulse, namely 250N, 500N, 750N and 1000N, which can be used to represent rocks with different compressive strengths, although the final applied pressure will be a function of the drill-bit geometry.

The measured effective impulse delivered above these four force thresholds in experiments are shown in **Fig. 7**. An increase in the force threshold naturally causes a significant reduction in the delivered effective impulse. However, as the weight-on-bit increases, the delivered effective impulse shows a slight growth due to an increase in the hammering frequency from 28Hz to around 37Hz for the full wavelength drill tool, and from 47Hz to 50Hz for the half wavelength drill tool. The effective impulse appears less sensitive to the change in the rate of front spring k_f than to change in the rate of rear spring k_r.

The most important conclusion from this figure is that, in comparison with the half wavelength percussive drill, the full wavelength drill tool delivers higher impulse over the same set of mechanical parameters considered in this study. This is because the greater momentum of the larger mass of the full wavelength drill tool produces slightly higher force peaks during percussion against the impact plate.

It should be emphasized that the experimental results shown in **Fig. 7** represent the effective impulse, which is often considered to be a predictor of the real percussive drilling performance [6]. However, many other factors may affect the in-situ drilling performance, including rock-related parameters, drill rotation speed, and debris removal speed [13].

4. Finite Element Analysis (FEA) of the ultrasonic percussive stacks

The FEA models of the full and half wavelength ultrasonic percussive stacks are shown in **Fig. 8**. Both consist of an ultrasonic transducer, a toroidal 6g free-mass, a free-mass holder to align the free-mass during percussion, an 80g hollow drill-bit and an impact plate. These parts are all made from Grade 5 Ti-6Al-4V titanium alloy. In addition, a rear plate and a front plate made from aluminium alloy 6082-T6 are employed to accommodate the rear and front compression springs. The interactions between the horn tip, free-mass, drill-bit tip and impact plate are defined as 'hard' and 'frictionless' contacts in FEA models. The impact plate has one side encastre as the boundary condition.

There are a number of options in FEA to represent a spring element, and in this study the connector option was employed, which models a spiral compression spring as a

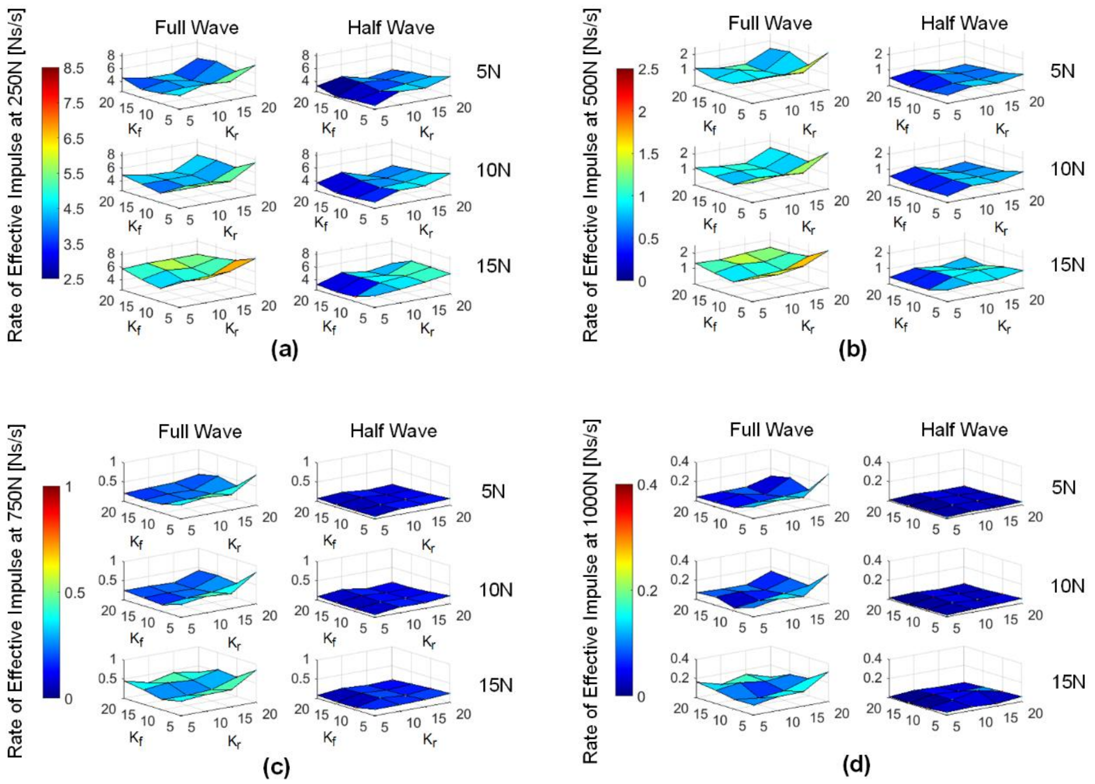

Fig. 7 Experimentally recorded effective impulse delivered above 250N, 500N, 750N and 1000N thresholds with weight-on-bit values of 5N, 10N and 15N for both full and half wavelength ultrasonic percussive stacks. (a) impulse above 250N, (b) impulse above 500N, (c) impulse above 750N, (d) impulse above 1000N

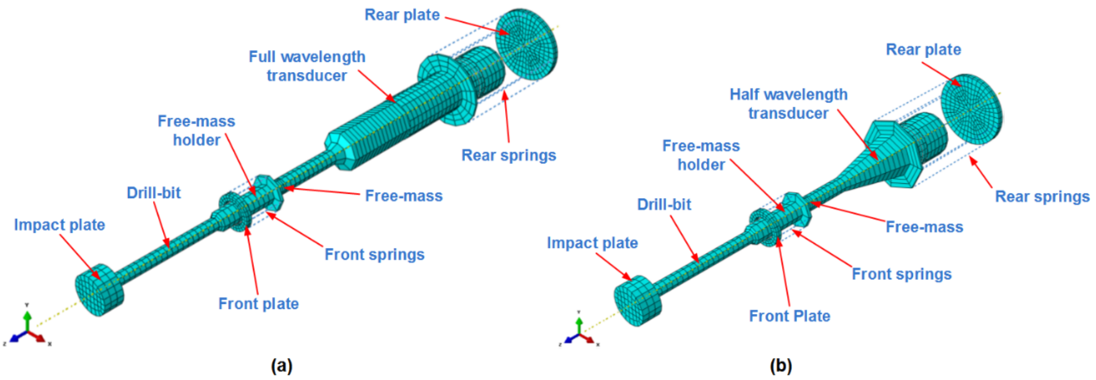

Fig. 8 Established ultrasonic percussive stacks in FEA: (a) full wavelength ultrasonic percussive stack, (b) half wavelength ultrasonic percussive stack

line connector that generates purely translational compression force. The spring rate and internal pre-load are easily defined.

Eight equal-stiffness compression spring equivalents are evenly distributed in parallel between eight nodes on the rim of the rear plane and eight nodes on the edge of transducer nodal flange (dashed lines in **Fig. 8**). The effective spring rate of these eight springs will be the rear spring rate used in experiments.

A similar arrangement is established to represent the front springs, which are accommodated between the rim of the front plane and the edge of the holder-mass flange (dashed lines).

The piezoceramic rings are modelled using 20-node quadratic elements, and the other components of the percussion models use 8-node linear elements. The 'implicit' algorithm has a calculation effort which is approximately proportional to n^2, where n is the number of degrees of freedom in the model [14].

Finally, a 6082-T6 aluminium housing connects the rear plate and front plate (hidden in **Fig. 8**). At the rim nodes of the housing, weight-on- bit values of 5N, 10N and 15N are applied, which are consistent with the experimental conditions. Due to the extremely high computation effort for the three-dimensional percussive models, it is impractical to simulate the percussion using the entire sets of front springs and rear springs. Instead, only one set combination is selected, which has a front spring rate $k_f = 5N/mm$ and a rear spring rate $k_r = 10N/mm$.

In order to allow the full wavelength transducer base vibration to reach 5 µm peak-to-peak during percussion, which further develops 40 µm peak-to-peak horn tip vibration, the magnitude of the applied voltage to the piezoceramic rings is set to 420V at a frequency of19833Hz. To drive the half wavelength percussive drill stack at the

This article has been accepted for publication in a future issue of this journal, but has not been fully edited. Content may change prior to final publication. Citation information: DOI 10.1109/TUFFC.2018.2867535, IEEE Transactions on Ultrasonics, Ferroelectrics, and Frequency Control

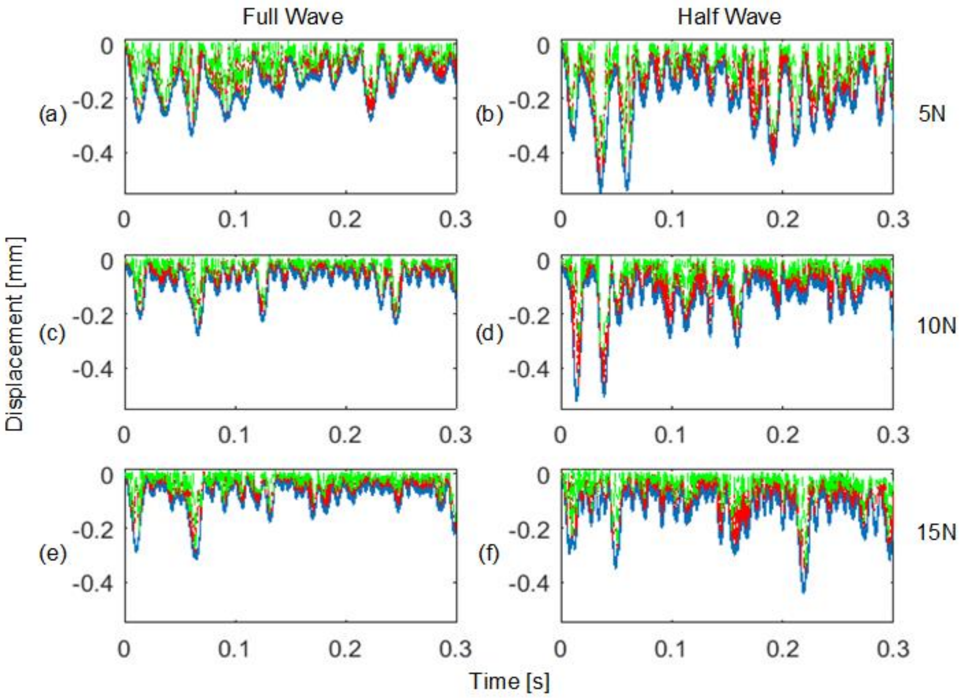

Fig. 9 Predicted displacements in FEA, with weights-on-bit as follows: (a) 5N full wave, (b) 5N half wave, (c) 10N full wave, (d) 10N half wave, (e) 15N full wave, (f) 15N half wave. Straight blue line – horn tip, dash-dotted red line – free-mass, dashed green line – free-mass holder

same power level, the magnitude of the applied voltage to the piezoceramic rings is adjusted to be 290V at a frequency of 19811Hz.

It is also important to consider the contact status when running the percussive drilling models. A small simulation step is required for a contact step but, for a non-contact sinusoidal vibration, a relatively large step is sufficient. A 'Dynamic Implicit' step is used which considers the piezoelectric effect as the excitation input, and a 0.3-second time interval is defined to study the percussive behaviour. A time step of 3.38×10^{-6}s is sufficient for non-contact and a time step of 6.33×10^{-7}s is required for contact. The simulation is completed after around 88000 load steps. Computation was performed on High Performance Computing (HPU) servers (2×14 core Intel Xeon E5-2697 v3 CPUs, 256GB RAM, CentOS 6.7 operating system).

4.1 Displacements of horn tip, free-mass and free-mass holder

Results of the displacement of horn tip, free-mass and free-mass holder are shown in **Fig. 9**. The displacements are averages of the nodal outputs on the horn tip face, free-mass body, and free-mass holder face.

For all six scenarios, the free-mass oscillates chaotically and every impact with the free-mass holder, and therefore the impact plate, is recorded as a force peak. The half wavelength ultrasonic percussive stack presents a slightly larger vibration displacement magnitude in comparison with the full wavelength percussive stack, as a result of the lighter mass. The overall response shares a high similarity with the vibrations measured using high speed cameras in related studies [6].

4.2 Percussive hammering force

The FEA-predicted percussive impact force and measured hammering force are presented in **Fig. 10**.

As the applied weight-on-bit increases, the hammering force increases in both simulation and experiment. The hammering force frequency increases from 33Hz to 42Hz for the simulated full wavelength model, and in experiment the frequency grows from 32Hz to 35Hz. For the half wavelength model, the hammering force frequency increases from 51Hz to 60Hz, and this value increases from 48Hz to 53Hz for the experimentally recorded force. An increase in hammering force frequency results in a higher effective impulse.

The half wavelength drill tool is modelled as being capable of developing a higher vibrational displacement amplitude during percussion with the free-mass, which results in a similar impact force level to the full wavelength percussive stack in spite of its lower mass.

Generally, the predicted hammering force peak magnitude is comparable to the experimentally recorded force. It should be noted that no effective impulse is calculated based on the predicted hammering force in FEA, because an excessively long percussion time window is required to obtain a reliable effective impulse value for different force thresholds.

4.3 Impact-induced stress

The predicted maximal Von Mises stresses of horn tip, free-mass and free-mass holder (drill-bit base) for both ultrasonic percussive drill tool models in FEA within a simulation period of 0.3-second are presented in **Fig. 11**. The maximal Von Mises stress tends to occur at the free-mass holder for both drill tool models. As the applied weight-on-bit increases, the stress level also rises.

The half wavelength ultrasonic percussive stack develops a considerably higher stress than the full wavelength drill tool, which in turn results in a higher collision force. This again

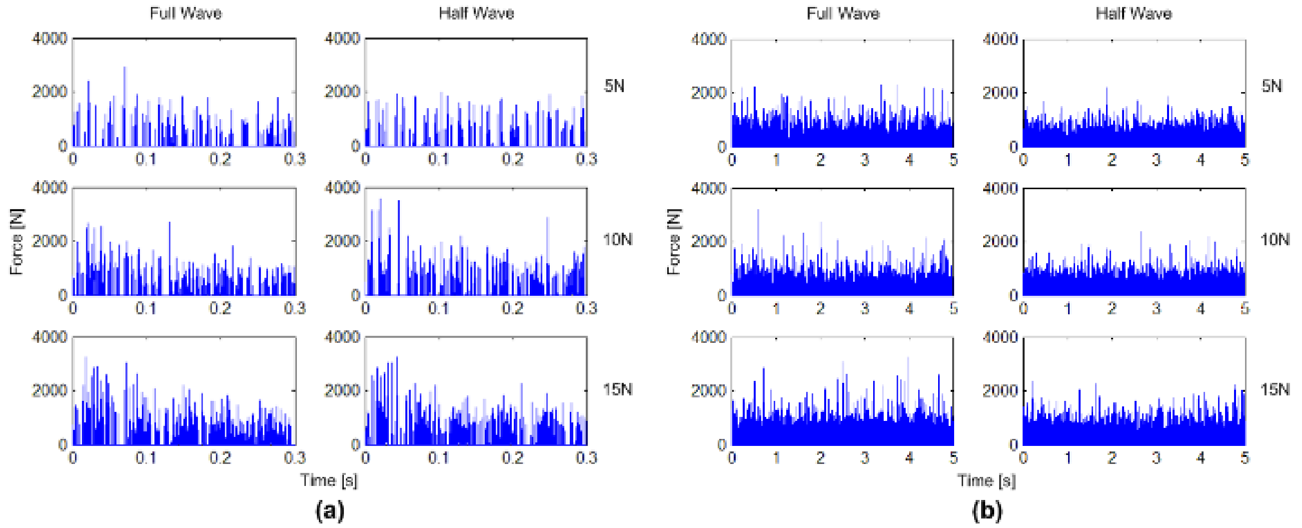

Fig. 10 (a) Predicted percussive hammering force in FEA and (b) experimentally measured percussive hammering force, for both full and half wavelength drill tools varying weight-on-bit values

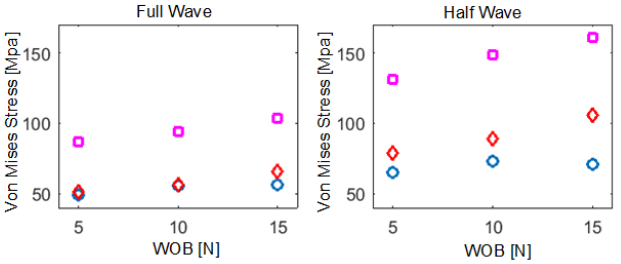

Fig. 11 FEA-predicted maximal Von Mises stress of horn tip, free-mass and free-mass holder with different weight-on-bit levels for the full wave and half wavelength drill tools during percussion. o – horn tip, ◊ – free-mass, ☐ – free-mass holder

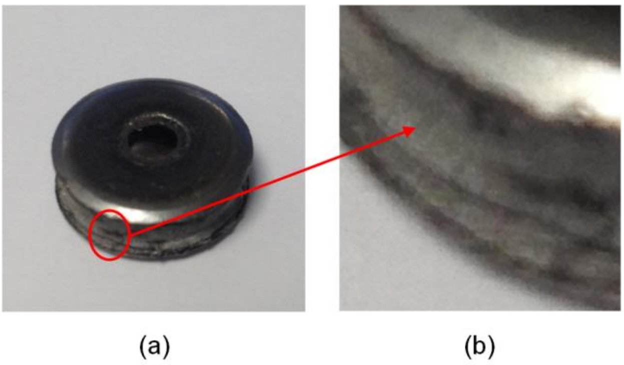
(a) (b)

Fig. 12 (a) Severely deformed free-mass for a long period of percussion, (b) detailed deformation

explains why there is hardly any difference observed in the percussive hammering force, regardless of the significant difference in the mass between two drill tools, as shown in **Fig. 11**.

In order to assess the wear experienced by the mechanical parts, **Fig. 12** is presented. After a sufficiently long period of percussion, the free-mass was significantly shortened and deformed. This suggests a stronger material should be used for any campaign drill tool.

5. Rock drilling with both percussive drill tools

Rock drilling experiments were carried out to further support the findings of the experimental study in section **3**, namely that the full wavelength drill tool offers a superior drilling performance in different types of rock. Three types of sandstone were used: Locharbriggs sandstone, Cullalo sandstone, and Clashach sandstone, representing medium, medium-hard and hard materials. The material properties of these three rocks are shown in **Table I**.

The experimental test rig was established as illustrated in **Fig. 5**. The drill tools are pulled horizontally by two parallel sets of attached weights via two pulley wheels, to provide 5N, 10N and 15N weight-on-bit values. A 6g free-mass is used. The front spring rate is $k_f = 5N/mm$ and rear spring rate is $k_r = 10N/mm$, which are consistent with the parameter settings applied in the FEA models. A 5µm peak-to-peak vibration amplitude for the full wavelength transducer radiating face is selected. As before, to achieve the same power consumption as the transducer vibrating in air, the half wavelength transducer displacement is set as 5.9µm peak-to-peak. The internal pre-load is set to 10N for the full wavelength drill tool, and the pre-load for the half wavelength drill tool is carefully adjusted to match the power of full wavelength drill tool during percussion in air.

A linear position sensor (PS-C15M-200) is mounted axially between the drill tool bottom plate and the stanchion, to measure the absolute displacement of the drill tool advancement. A rock sits on an L-shaped table which is attached to the stanchion. The motor rotation is set to 15rpm and each session of drilling takes around 10 minutes.

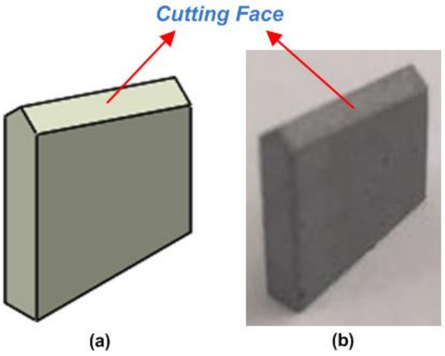

Fig. 13 Cutting tooth for rock drilling/coring. (a) as-designed tooth, (b) manufactured tooth.

Fig. 13 illustrates the cutting teeth used for the rock drilling tests. Each triangular shaped cutting tooth, made from Tungsten-Carbide (TC) grade NF11, consists of two cutting

Table I. Sandstone material properties

Rock Type	**Locharbriggs**	**Cullalo**	**Clashach**
UCS [MPa]	44 [16]	50 [17]	132
Density [kg/m^3]	2210	2160	2084
Porosity [%]	26.0	18.4	21.4
Water Absorption [%]	9.3	11.2	6.9

faces and a chisel edge. The dimension of each cutting tooth is 6.3mm × 6.6mm × 1.3mm.

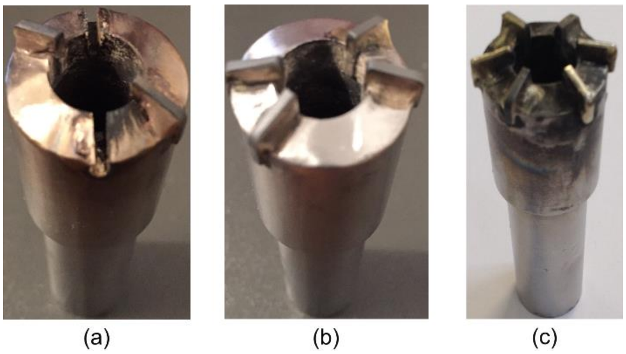

(a) (b) (c)

Fig. 14 Drill head: (a) two teeth (although slotted for four), (b) four teeth, (c) six teeth

The drill heads used to perform the rock drilling/coring experiments are illustrated in **Fig. 14**. The driller/corer is cylindrical, weighs 60g, and is made from Grade 5 Ti-6Al-4V titanium alloy with a hollow hole in the centre. The corer has an overall length of 80mm, an outer diameter of 20mm, and hole diameter of 10mm [15].

The influence of the contact area on the drilling progress is also studied, by using configurations with 2 teeth, 4 teeth and 6 teeth, corresponding to impact areas of 17mm^2, 34mm^2 and 51mm^2 respectively, calculated from the dimension of the cutting tooth in **Fig. 13**.

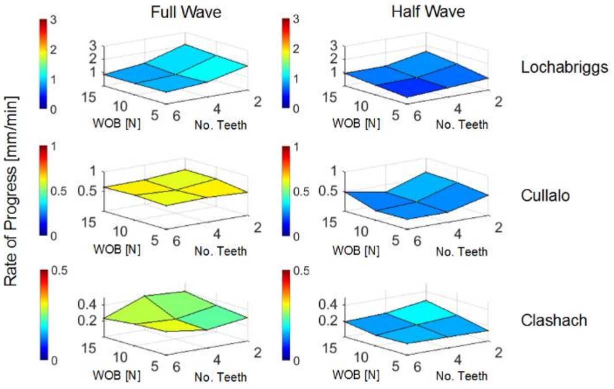

Fig. 15 Rate of progress of the drill tools in Locharbriggs sandstone, Cullalo sandstone, and Clashach sandstone.

Fig. 15 shows the results of the rate of progress for both ultrasonic percussive drill tools in three types of sandstones. An increase in the weight-on-bit had no significant influence on the drilling progress for both drill tools, in spite of the change in rock hardness and number of teeth used. However, a reduction in contact area between the cutting teeth and the rock surface increases the drilling progress, especially during drilling into medium hardness sandstone. Also, as the rock hardness increases, the drilling progress decreases, which is expected.

In general, however, it appears that when compared to the half wavelength drill tool, the full wavelength drill tool yields only slightly faster progress despite the significant differences in effective impulse between the two systems presented in **Fig. 7**.

Table II. Full wavelength percussive rock drilling

Rock Type	**Image**	**Depth [mm]**	**RoP [mm/min]**
Locharbriggs sandstone		19.88	2.095
Cullalo sandstone		7.14	0.713
Clashach sandstone	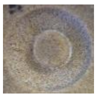	4.04	0.400

Table III. Half wavelength percussive rock drilling

Rock Type	**Image**	**Depth [mm]**	**RoP [mm/min]**
Locharbriggs sandstone		16.15	1.567
Cullalo sandstone		6.49	0.648
Clashach sandstone	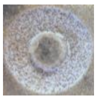	3.22	0.288

Some boreholes generated in the three types of sandstones when a 2 teeth cutting head and 15N weight-on-bit were employed are presented in **Table II** and **Table III.**

6. Conclusion

A 3-D transient FEA model of full wavelength and half wavelength electromechanical transducers in FEA is presented and validated by experimental measurements.

Dynamic analysis and parametric optimization on the compression springs rates for both drill tools are performed, which suggest a stronger rear spring and a weaker front spring should be used when building a drill tool, as this results in the highest level of effective impulse for different force thresholds that represents the hardness of rocks. Using a similar input power to the ultrasonic transducers, the full wavelength drill tool tends to develop a higher effective impulse than the half wavelength drill tool.

The actual rock drilling experiments were executed in order to confirm the superiority of the full wavelength drill tool. These were conducted on medium, medium-hard and hard rocks with different weight-on-bit values. Furthermore, the contact area between the drill head and rock surface was also studied to understand impact pressure effect on the rate of drilling/coring progress.

Interestingly, the recorded rate of progress for the full wavelength drill tool fails to present an excellent performance compared with the half wavelength drill tool. Within a 10 minutes drilling session, the absolute depth achieved by both drill tools were quite similar. The reasons for these results are still unknown.

Based on the results achieved in this paper, the half wavelength ultrasonic transducer is preferred due to its comparable dynamic behaviour at an almost 30% saving in mass, but the mechanism underlying its unexpectedly good performance remains to be explained.

Acknowledgement

The authors acknowledge the use of the High Performance Computing facilities and support service within the School of Engineering, University of Glasgow.

References

[1] X. Bao, Y. Bar-Cohen, Z. Chang, B. P. Dolgin, S. Sherrit, D. S. Pal, S. Du, and T. Peterson, “Modeling and computer simulation of ultrasonic/sonic driller/corer (USDC),” *IEEE Transactions on Ultrasonics, Ferroelectrics and Frequency Control*, vol. 50, no. 9, pp. 1147-60, Sep. 2003.

[2] Y. Bar-cohen, S. Sherrit, B. P. Dolgin, X. Bao, Z. Chang, S. Dharmendra, R. Krahe, J. Kroh, S. Du, and T. Peterson, “Ultrasonic/sonic drilling/coring (USDC) for planetary applications,” in *Proceedings of SPIE's 8th Annual International Symposium on Smart Structures and Materials*, no. 4327, pp. 5-8, 2001.

[3] S. Sherrit, S. A. Askins, M. Gradziol, B. P. Dolgin, X. Bao, Z. Chang, and Y. Bar-cohen, “Novel Horn Designs for Ultrasonic/Sonic Cleaning Welding, Soldering, Cutting and Drilling,” in *Proceedings of the SPIE Smart Structures* Conference, vol. 4701, no. 34, 2002.

[4] K.-M. Shu, W.-H. Hsieh, and H.-S. Yen, “on the Design and Analysis of Acoustic Horns for Ultrasonic Welding,” in *Transactions of the Canadian Society for Mechanical Engingeering*, vol. 37, no. 3, pp. 905-916, 2013.

[5] Y. Bar-Cohen, S. Sherrit, B. P. Dolgin, N. Bridges, X. B. X. Bao, Z. C. Z. Chang, a. Yen, R. S. Saunders, D. Pal, J. Kroh, and T. Peterson, “Ultrasonic/sonic driller/corer (USDC) as a sampler for planetary exploration,” in *2001 IEEE Aerospace Conference on the Topic of “Missions, Systems, and Instruments for In-Situ Sensing*,” vol. 1, pp. 1-10, 2001.

[6] P. Harkness, M. Lucas, and A. Cardoni, “Maximization of the Effective Impulse Delivered by a High-Frequency/Low-Frequency Planetary Drill Tool,” in *IEEE Transactions on Ultrasonics, Ferroelectrics, and Frequency Control*, vol. 58, no. 11, 2011.

[7] R. Timoney, P. Harkness, K. Worrall, X. Li, a Bolhovitins, and Lucas, “The Development of the European Ultrasonic Planetary Core Drill (UPCD),” in *Space Conference & Exposition, AIAA Space 2015*, pp. 1-11, 2015.

[8] K. Worrall, R. Timoney, P. Harkness, X. Li, and M. Lucas, “Ultrasonic Planetary Core Drill: Overview and Results from Field Trial,” in *14th Symposium on Advanced Space Technologies in Robotics and Automation*, pp. 1-8, 2017.

[9] X. Li, P. Harkness, K. Worrall, R. Timoney, and M. Lucas, “A parametric study for the design of an optimized ultrasonic-percussive planetary drill tool,” in *IEEE Transactions on Ultrasonics, Ferroelectrics, and Frequency Control*, 64(3), pp. 577-589, 2017.

[10] D. Berlincourt, H. Krueger, and C. Near, “Properties of Morgan electro ceramic ceramics,” *Technical Publication TP-226 Properties of Piezoelectricity Ceramics*, pp. 1-12, 2000.

[11] P. Avitabile, “Experimental Modal Analysis,” *Modal Analysis and Controls Laboratory, University of Massachusetts Lowell, raft document for Sound & Vibration Magazine*, vol. 35, no. 1, pp. 1-15, 2001.

[12] H. Al-Budairi, “Design and analysis of ultrasonic horns operating in longitudinal and torsional vibration,” *University of Glasgow, School of Engineering, Enlighten PhD Theses*, pp. 115, December, 2012.

[13] M. Badescu, S. Sherrit, X. Bao, Y. Bar-Cohen, and B. Chen, “Auto-Gopher: A Wire-Line Rotary-Hammer Ultrasonic Drill,” in *Proceedings of SPIE Smart Structures and Materials* Conference, vol. 7981, March, 2011.

[14] C. Potthast, J. Twiefel, and J. Wallaschek, “Modelling approaches for an ultrasonic percussion drill,” in *Journal of Sound and Vibration*, vol. 308, no. 3-5, pp. 405-417, March, 2007.

[15] R. Timoney, X. Li, K. Worrall, P. Harkness, and M. Lucas, “Push-and-Twist Drillstring Assemblies,” in *ACSE Earth and Space 2016*. pp. 1-12, 2016.

[16] “Physical Performance of Geomembranes,” *Datasheet of Locharbriggs Permian Sandstone,*

no. 509579, 2013.

[17] S. Barr, W. J. McCarter, and B. Suryanto, "Bond-strength performance of hydraulic lime and natural cement mortared sandstone masonry," *Construction and Building Materials*, vol. 84, pp. 128-135, 2015.